Editors' Suggestion | Featured in Physics

Phason-Dominated Thermal Transport in Fresnoite

M. E. Manley,[1,*] A. F. May,[1] B. L. Winn,[2] D. L. Abernathy,[2] R. Sahul,[3] and R. P. Hermann[1]
[1]Material Science and Technology Division, Oak Ridge National Lab, Oak Ridge, Tennessee 37831, USA
[2]Neutron Scattering Division, Oak Ridge National Lab, Oak Ridge, Tennessee 37831, USA
[3]Amphenol Corporation, Frederick, Maryland 21701, USA

(Received 20 January 2022; accepted 20 October 2022; published 14 December 2022)

Fast-propagating waves in the phase of incommensurate structures, called phasons, have long been argued to enhance thermal transport. Although supersonic phason velocities have been observed, the lifetimes, from which mean free paths can be determined, have not been resolved. Using inelastic neutron scattering and thermal conductivity measurements, we establish that phasons in piezoelectric fresnoite make a major contribution to thermal conductivity by propagating with higher group velocities and longer mean free paths than phonons. The phason contribution to thermal conductivity is maximum near room temperature, where it is the single largest contributing degree of freedom.

DOI: 10.1103/PhysRevLett.129.255901

Introduction.—Crystals with incompatible translational periodicities, where two or more periodic spacings cannot be expressed as a ratio of integers, are described as incommensurate. In such crystals the accumulating phase difference between incommensurate periodicities can be described in terms of a regular lattice of solitons [1–3]. The existence of such incommensurable elements also introduces associated quasiparticle excitations called phasons and amplitudons [3]. Phasons are high velocity acousticlike modes in the soliton lattice and amplitudons are opticlike excitations in the amplitude of the solitons with typically lower velocities. Phasons are anticipated to play an important role in transport [4,5] and anomalous contributions to thermal conductivity in incommensurate charge-density-wave systems have been attributed to high velocity phasons [6,7]. Furthermore, phasons with group velocities much larger than phonons have been observed for both incommensurate charge-density waves in blue bronze [8] and in incommensurately modulated piezoelectric fresnoite ($Ba_2TiSi_2O_8$) [9]. By contrast, more recent work on complex materials for energy applications have argued that the appearance of incommensurate structure suppresses thermal conductivity [10,11]. The generality of such a claim needs to account for the impact of the additional lattice degrees of freedom that exist in incommensurate crystals. Hence, there is a need to quantify the role of phasons in thermal transport. However, to fully establish the importance of phasons for thermal conductivity it is crucial to also determine and compare the phason and phonon mean free paths (MFP).

In the phonon or phason gas model, the thermal conductivity is expressed as the sum [12]

$$\kappa = \frac{1}{3}\sum_{\boldsymbol{q}s} C_{\boldsymbol{q}s} v_{\boldsymbol{q}s} l_{\boldsymbol{q}s}, \tag{1}$$

where the products of mode specific heat capacity $C_{\boldsymbol{q}s}$, group velocity $v_{\boldsymbol{q}s}$, and MFP $l_{\boldsymbol{q}s}$, are summed over momentum $\boldsymbol{q}$ for all s branches. Phason group velocities can be much higher than that of phonons [8,9]. However, the phason mode specific heat capacity is always smaller because phonons and phasons are divided up among the atomic vs the soliton degrees of freedom, and the latter contains *groups* of atoms. For fresnoite, the heat capacity per phason branch is about one sixth that of acoustic phonons [9]. The MFP remains an unknown deciding factor in determining the balance of phason vs phonon thermal conductivity.

Though phasons are governed by the same thermal population statistics as phonons, they manifest differently in the thermal conductivity, which we use to isolate the phason contribution. First, because incommensurate modulations are usually confined to certain crystallographic directions, the associated phason contribution to thermal conductivity can be separated by crystallographic direction. Second, the MFP of low-energy phonons becomes very large at cryogenic temperatures and results in a dominant peak in thermal conductivity [12] whereas the corresponding phasons are always diffusive at sufficiently long wavelengths [13,14], and this results in a vanishingly small contribution at cryogenic temperatures [6]. Third, phasons necessarily vanish, although gradually [9], when the crystal transitions to a commensurate phase, typically at high temperatures. Considering these trends, we selected fresnoite as an ideal material for isolating the phason thermal conductivity. Fresnoite is a promising piezoelectric material for sensor applications [15,16] that develops a two-dimensional incommensurate structural modulation in the basal plane of its noncentrosymmetric tetragonal phase (space group $P4bm$) on cooling below ~433 K [17,18]—although phasons first emerge gradually as a precursor starting below

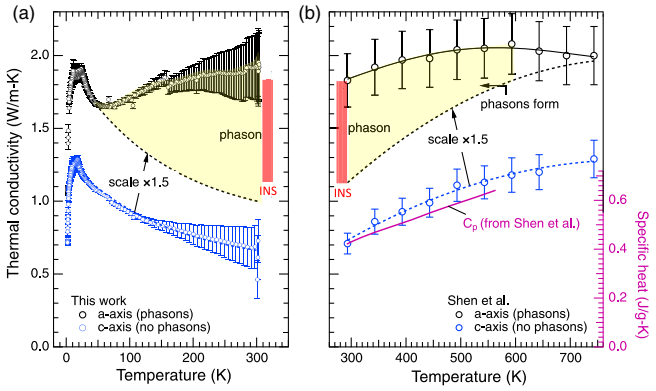

FIG. 1. Thermal conductivity of fresnoite measured along the tetragonal a axis (with phasons) and c axis (without phasons). (a) Low temperature thermal conductivity measured using a four-point method (this work). (b) High temperature thermal conductivity measured using the laser flash technique along with heat capacity measurements both by Shen *et al.* [16].

~600 K [9]. Phasons in fresnoite are confined to the basal plane and vanish on heating above ~600 K. Importantly, fresnoite does not have an electronic contribution to the thermal conductivity.

Here, we combine anisotropic thermal conductivity measurements with high-resolution inelastic neutron scattering measurements of the phason and phonon dispersions and line shapes to establish that phasons make a major contribution to the thermal conductivity of fresnoite. The results clearly demonstrate that phasons dominate the thermal conductivity within the basal plane near room temperature, and therefore provide a clear explanation for the enhanced anisotropy observed in transport measurements.

Thermal conductivity.—To estimate phason transport below room temperature, thermal conductivity was measured using the Quantum Design Thermal Transport Option in a physical property measurement system. Crystallographic orientations of two crystals were confirmed using two-theta scans on a PANalytical X'Pert Pro MPD with Cu K_α radiation ($\lambda = 1.5406$ Å). A four-point method was employed using gold coated copper leads attached to the crystals with EPO-TEK H20E silver epoxy; an effort was made to utilize samples of similar dimensions. Figure 1(a) shows the thermal conductivity along both the a axis and c axis of tetragonal fresnoite [17]. As expected, thermal conductivity along the c axis shows the trend expected for phonons; an inverse power-law increase on cooling from reduced phonon-phonon scattering leading to a peak at ~15 K, below which it decreases rapidly [12]. Along the a axis thermal conductivity behaves similarly below ~50 K, but then shows a minimum on heating followed by a gradual increase up to room temperature, Fig. 1(a). This behavior is characteristic of phasons [6], where the phason contribution vanishes at low temperatures because the lowest energy phasons are intrinsically damped [13,14], and then rises as the longer-lived phasons thermally populate at higher temperatures. The phason contribution [highlighted yellow in Fig. 1(a)] along the a axis is estimated by fitting the phonon contribution along the c axis and scaling the result by a factor of 1.5 to match the bare phonon behavior below 50 K (the scale factor is reasonable since it reflects the anisotropy in the elastic stiffness and therefore acoustic phonon velocities, e.g., $c_{11}/c_{33} = v^2_{[100]L}/v^2_{[001]L} = 1.65$ [19]). This analysis predicts a phason contribution of ~1 W m^{-1} K^{-1} or half of the total thermal conductivity at 300 K, comparable to that of phasons associated with charge density waves [6]. This same procedure (and scale factor) was also applied at high temperature for thermal conductivity along the a axis and c axis by Shen *et al.* [16], see Fig. 1(b). The estimate for the phason contribution at 300 K of about ~1 W m^{-1} K^{-1} is the same within error. The phason contribution vanishes again ~600 K, near where the phasons vanish according to inelastic neutron scattering [8]. The gradual increase in thermal conductivity above room temperature along the a axis closely scales with the measured heat capacity from the same study [16] [Fig. 1(b)]. This behavior is not expected for a normal phonon gas but is consistent with possibly a third contribution from diffusons, which was shown to be important in complex crystals when there is sufficient overlap between numerous phonon branches [20,21]. We now turn to inelastic neutron scattering to explore these contributions in more detail.

Cold inelastic neutron scattering.—To determine the phason and phonon dispersion curves and line shapes, inelastic neutron scattering from a 25 cm^3 fresnoite single crystal was collected with the cold neutron time-of-flight hybrid spectrometer HYPSEC [22] at the Spallation Neutron Source (SNS) at Oak Ridge National Laboratory. The instrument was operated in two configurations: first with an incident energy $E_i = 15$ meV (360 Hz chopper), and then with $E_i = 7.5$ meV (300 Hz chopper) with a 20' Soller collimator added for increased momentum, $\boldsymbol{Q}$, resolution. The best possible $\boldsymbol{Q}$ resolution is needed to determine the linewidth of the phason at the steepest part of the dispersion curve. At $E_i = 15$ meV a volume of data in $\boldsymbol{Q}$-E space was generated by rotating the [100] axis with respect to the incident beam in 0.25° steps from 0° to 85°, and at $E_i = 7.5$ meV the rotation was in 0.125° steps from −22° to 10°. The data were analyzed using MSlice in the Data Analysis and Visualization Environment (DAVE) software [23]. Figure 2(a) shows the 2D-diffraction pattern, which contains both the commensurate reflections (integer indices), from which the acoustic phonons emerge and the incommensurate reflections, from which phasons emerge. The intensity image plots in Figs. 2(b) and 2(c) show examples of phonons and phasons, respectively. Because the phason dispersion curve is so steep [Fig. 2(c)], the ability to resolve the line shape was limited by the $\boldsymbol{Q}$ resolution rather than the energy resolution, especially

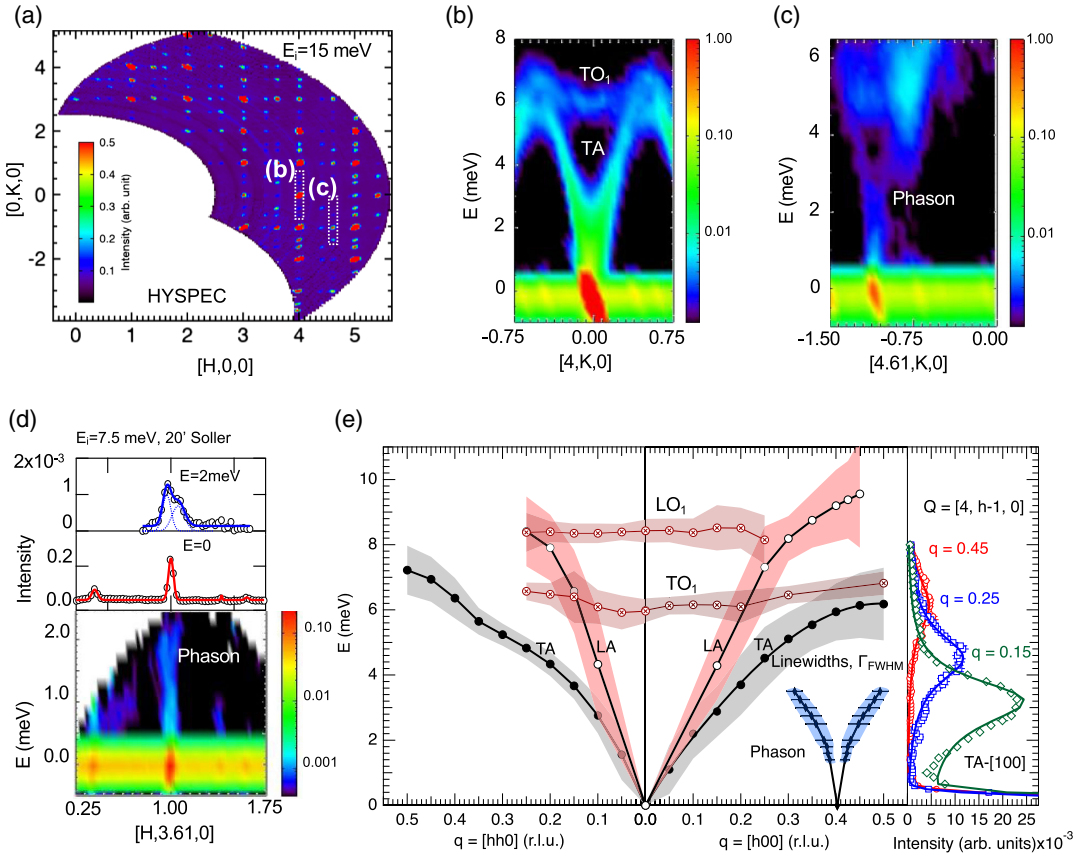

FIG. 2. Phason and low-energy phonon dispersion and linewidths measured in the basal plane of fresnoite using the HYSPEC time-of-flight cold neutron instrument at the SNS. (a) Intensity map of the elastic scattering for data collected with $E_i = 15$ meV. (b) Slice in energy of the same data along $\boldsymbol{Q} = [4, \mathrm{K}, 0]$ through a commensurate reflection, revealing transverse acoustic (TA) and optic (TO_1) phonons. (c) Slice in energy along $\boldsymbol{Q} = [4.61, \mathrm{K}, 0]$ through an incommensurate reflection, revealing the phason. The out-of-plane directions were integrated ± 0.05 r.l.u. for the slices displayed in (a) and (c). (d) Measurement of lower energy part of phason along $\boldsymbol{Q} = [\mathrm{H}, 3.61, 0]$ using $E_i = 7.5$ meV and 20' Soller collimation for significantly improved energy and momentum resolution. Constant energy cuts in top panels show the resolution limited elastic peak at $E = 0$ and the broader phason at $E = 2$ meV. The out-of-plane directions were integrated ± 0.025 r.l.u. for the slices and cuts displayed in (d). (e) Summary of the phason and low-energy phonon dispersion with linewidths along the [100] and [110] directions. Shading indicates the intrinsic full width at half maximum (FWHM) found by fitting with Lorentzian convoluted with a small Gaussian instrument resolution width; example fits shown in right panel. All phonons are fit in energy at fixed $\boldsymbol{Q}$, while the phason widths are fit in $\boldsymbol{Q}$ at fixed E.

below 2.5 meV. For this reason, the shapes were determined by cutting the data along $\boldsymbol{Q}$ and fitting a series of constant energy cuts. Below 2.5 meV the necessary $\boldsymbol{Q}$ resolution was even tighter and required the switch to 7.5 meV incident energy with 20' Soller collimation [Fig. 2(d)]. In this configuration the observed phason width at 2 meV (0.08 ± 0.01 r.l.u.) is many times larger than the width of the resolution limited elastic peak width (0.028 ± 0.001 r.l.u.), see top panels in Fig. 2(d). Figure 2(e) provides a summary of the acoustic phonon and phason dispersion curve and linewidth measurements. Two low-lying optic phonons, TO_1 and LO_1, were also detected. They have little impact on thermal conductivity since they have near zero group velocities. Intrinsic linewidths for all peaks were determined by fitting to a Lorentzian convoluted with a Gaussian resolution function. The transverse acoustic (TA) and longitudinal acoustic (LA) phonons have energy widths [shaded regions around curves in Fig. 2(a)] mostly in the 1-to-2 meV range, much larger than the instrument resolution. The nominal instrument resolution varies—it ranges from 0.16 meV at 10 meV to 0.4 meV at the elastic line, and from 0.08 meV at 6 meV to 0.2 meV at the elastic line, for $E_i = 15$ meV and 7.5 meV, respectively. For transverse branches a tilt in the resolution function results in resolution focusing, which was also included (see Supplemental Material, Figs. S1 and S2 [24]). The resolution corrected linewidths were all cross checked against observations of the same modes in different zones and/or with different instrument configurations.

The MFPs of the phonons and phasons can be expressed in terms of quantities readily deduced from the dispersion curves and linewidths [25],

$$l_{qs} = v_{qs}\frac{\hbar}{\Gamma_{qs}}, \tag{2}$$

where the group velocity v_{qs} is from the slope of the dispersion curve, and Γ_{qs} is the energy full width at half maximum of the dispersion curve. Thus, the narrower and steeper the dispersion the longer the MFP (or, when v_{qs} and Γ_{qs} vary slowly, the inverse of the width in $\boldsymbol{Q}$, the coherence length, is also approximately the MFP). On inspection of Fig. 2(e), phasons are both narrower and steeper than phonons, indicating that they have longer MFPs. The MFPs for the phason dispersion ranges from ~7 to 14 nm—14 nm near the lower (<2 meV) and 7 nm in the upper part of the curve (3 to 4 meV). The phasons are isotropic in the basal plane [9]. For comparison, the [100]-TA phonon and the [100]-LA phonon have an MFP of only 3 nm over the bulk of the curve between 2 and 5 meV and an MFP of about 4 nm in the same range, respectively. The [110]-LA and the [110]-TA have an MFP of 3.2 nm and 3 nm at 4.5 meV, respectively. Hence, the phason MFPs are on average about 3 times larger than those of the acoustic phonons propagating in the same plane. The group velocities of the phasons are also ~2.8 to 4.3 times higher than the acoustic phonons whereas their density of states (and mode specific heat capacity at ambient conditions) is about 6.25 times less [9]. Appropriately weighing these factors together with the MPFs in Eq. (1), the phason contribution to the thermal conductivity in the basal plane is about 2.5 times larger than the [100]-TA acoustic phonon (see Supplemental Material Fig. S3 [24]). The absolute value of the phason contribution at 300 K can also be estimated from the average group velocities and MFPs and works out to be about 0.7 $\mathrm{W\,m^{-1}\,K^{-1}}$ [24], which is consistent with the value deduced from the thermal conductivity measurements (Fig. 1). Hence, this analysis also indicates that ~50% of the thermal conductivity along the a axis at 300 K comes from phasons. In addition to the acoustic-phonon contribution there are also optic phonons, optic-mode-like amplitudons, or diffusons. Although these modes tend to have lower propagation velocities (flatter dispersion) they dominate the lattice density of states in crystals as complex as fresnoite. These numerous modes also exhibit considerable overlap in momentum and energy, making them difficult to separate in a single crystal measurement. However, the distribution of these modes can be probed in a powder measurement of the lattice density of states.

Epithermal inelastic neutron scattering.—The full lattice dynamical spectrum of fresnoite was measured on 30 grams of powder using the ARCS time-of-flight instrument at the SNS of Oak Ridge National Laboratory [26]. To reach the highest energy optic phonons the instrument was operated with an incident neutron energy of 120 meV. The powder was contained within a thin-walled aluminum can mounted in a closed-cycle displex refrigerator for measurements at 5 K. The measured spectra were corrected for sample background by measuring and subtracting the scattering from an identical empty aluminum can. The powder average scattering function, $S(|Q|, E)$, was then determined by correcting for the k_i/k_f phase space factor. A neutron-weighted density of states was extracted by summing the measured $S(|Q|, E)$ over large volume of momentum space including numerous zones from 2 to 12 $\mathrm{Å^{-1}}$, subtracting the elastic peak and the incoherent multiphonon contribution calculated iteratively to all orders [27–29], and correcting for the thermal occupation and Debye-Waller factors. Figure 3 shows the neutron-weighted density of states [Fig. 3(a)] and the scattering function [Fig. 3(b)]. The upper most optic phonons cut off just below about 100 meV. As indicted in Fig. 3(a), the phasons and acoustic phonons cut off at energies well below most of the density of states, which is primarily made up of optic phonons. Nevertheless, the low energy modes dominate the thermal

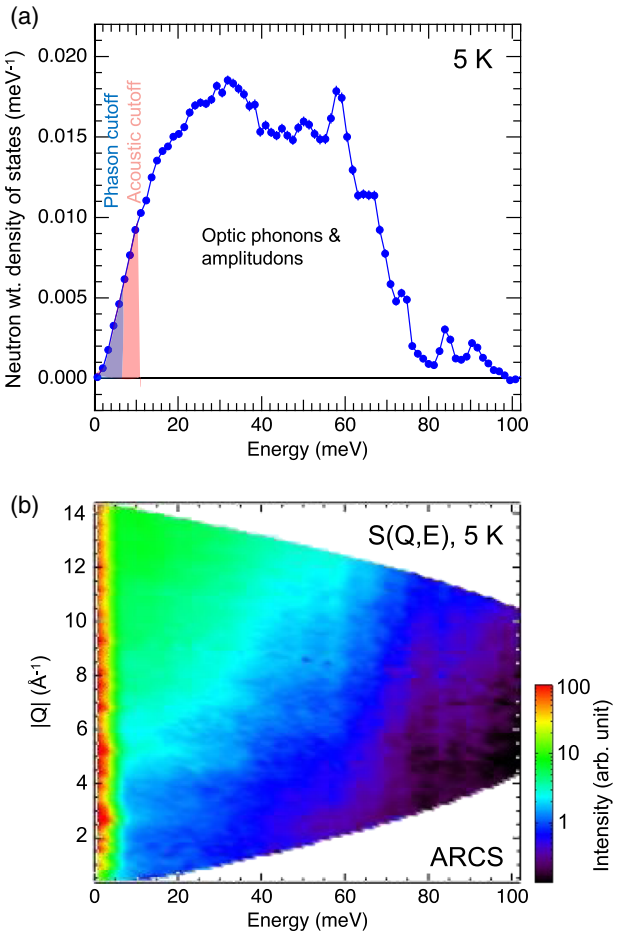

FIG. 3. Full neutron-weighted density of states and powder averaged dynamical structure factor at 5 K for fresnoite measured using the ARCS time-of-flight instrument at the SNS. (a) Extracted neutron-weighted density of states for the lattice dynamics that includes mainly phonons, but also phasons and amplitudons. (b) Intensity map of the powder averaged dynamical structure factor, $S(|Q|, E)$, from which the density of states was determined.

conductivity from ambient temperature and below. At the highest temperatures, however, the thermal population of the other modes is evident in the way the thermal conductivity along the c axis increases with the same scaling behavior as the heat capacity [Fig. 1(b)], which signals the expected increasing mode population [30]. This indicates a constant thermal diffusivity at the highest temperatures in Fig. 1, consistent with a diffuson channel, which comes about from a coupling of overlapping eigenstates [20,21,31–34]. Although the diffuson channel has traditionally been applied to disordered solids, recent work shows that in complex crystals where there is a high density of overlapping phonon branches it can also become important [20]. The scattering function of fresnoite shown in Fig. 3(b) indicates that the high-energy part of the density of states is composed of many flat modes, which is a situation that limits the phonon-gas channel and accentuates the diffuson channel in complex crystals [20]. Hence, the scattering function supports the notion that the slow rise in the thermal conductivity above 300 K along the c axis in Fig. 1(b) is most likely brought about by populating modes that provide a diffuson contribution. By extension, a diffuson contribution also likely rises beneath the diminishing phason contribution along the a axis in Fig. 1(b).

Conclusion.—Despite making a relatively small contribution to the lattice density of states, phasons make a major contribution to the thermal conductivity in the incommensurate phase of fresnoite by traveling faster and farther than the acoustic phonons. The phason contribution is anisotropic and reaches a maximum near ambient conditions, where it is the single largest contributor to thermal transport in the basal plane. At cryogenic temperatures the usual phonon-gas behavior dominates, while at high temperatures the phasons fade away and diffusons appear to make an important contribution. This work therefore establishes the importance of phasonic thermal conductivity and demonstrates that excitations unique to incommensurate lattices can dominate transport properties and must therefore be considered when attempting to model or optimize the behavior of such systems.

Neutron scattering by M. E. M. and R. P. H., and thermal conductivity measurements by A. F. M. were supported by the U.S. Department of Energy, Office of Science, Office of Basic Energy Sciences, Materials Sciences and Engineering Division under Contract No. DE-AC05-00OR22725. This research used resources at the Spallation Neutron Source, a DOE Office of Science User Facility operated by the Oak Ridge National Laboratory.

*Corresponding author.
manleyme@ornl.gov

[1] P. Bak and J. von Boehm, Ising model with solitons, phasons, and "the devil's staircase,", Phys. Rev. B **21**, 5297 (1980).
[2] P. Bak, Commensurate phases, incommensurate phases and the devil's staircase, Rep. Prog. Phys. **45**, 587 (1981).
[3] A. D. Bruce and R. A. Cowley, The theory of structurally incommensurate systems: III the fluctuation spectrum of incommensurate phases, J. Phys. C **11**, 3609 (1978).
[4] H. Fröhlich, On the theory of superconductivity: The one-dimensional case, Proc. R. Soc. A **223**, 296 (1954).
[5] J. D. Axe, Incommensurate structures, Phil. Trans. R. Soc. B **290**, 593 (1980).
[6] A. Smontara, K. Biljaković, and S. N. Artemenko, Contribution of charge-density-wave phase excitations to thermal conductivity below the Peierls transition, Phys. Rev. B **48**, 4329 (1993).
[7] X. Xu, A. F. Bangura, C. Q. Fiu, M. Greenblatt, S. Yue, C. Panagopoulos, and N. E. Hussey, Transport and thermodynamic properties of quasi-two-dimensional purple bronzes $A_{0.9}Mo_6O_{17}$ ($A = \mathrm{Na}$, K), Phys. Rev. B **85**, 195101 (2012).
[8] B. Hennion, J. P. Pouget, and M. Sato, Charge-Density-Wave Phase Elasticity of the Blue Bronze, Phys. Rev. Lett. **68**, 2374 (1992).
[9] M. E. Manley, P. J. Stonaha, D. L. Abernathy, S. Chi, R. Sahul, R. P. Hermann, and J. D. Budai, Supersonic propagation of lattice energy by phasons in fresnoite, Nat. Commun. **9**, 1823 (2018).
[10] N. Sato, H. Ouchi, Y. Takagiwa, and K. Kimura, Glass-like lattice thermal conductivity and thermoelectric properties of incommensurate chimney-ladder compound FeGeγ, Chem. Mater. **28**, 529–533 (2016).
[11] M. Beekman and D. G. Cahill, Inorganic crystals with glass-like and ultralow thermal conductivities, Cryst. Res. Technol. **52**, 1700114 (2017).
[12] N. W. Ashcroft and N. D. Mermin, *Solid State Physics* (Saunders College Publishing, New York, 1976) p. 500.
[13] A. Cano and A. P. Levanyuk, Explanation of the Glasslike Anomaly in the Low-Temperature Specific Heat of Incommensurate Phases, Phys. Rev. Lett. **93**, 245902 (2004).
[14] R. Zeyher and W. Finger, Phason Dynamics of Incommensurate Crystals, Phys. Rev. Lett. **49**, 1833 (1982).
[15] M. Kimura, Y. Fujino, and T. Kawamura, New piezoelectric crystal: Synthetic fresnoite ($Ba_2Si_2TiO_8$), Appl. Phys. Lett. **29**, 227 (1976).
[16] C. Shen, H. Zhang, H. Cong, H. Yu, and J. Wang, Investigations on the thermal and piezoelectric properties of fresnoite $Ba_2Si_2TiO_8$ single crystals, J. Appl. Phys. **116**, 044106 (2014).
[17] P. B. Moore and J. Louisnathan, Fresnoite: Unusual titanium coordination, Science **156**, 1361 (1967).
[18] T. Höche, C. Russel, and W. Neumann, Incommensurate modulations in $Ba_2TiSi_2O_8$, $Sr_2TiSi_2O_8$, and $Ba_2TiGe_2O_8$, Solid State Commun. **110**, 651 (1999).
[19] N. T. Taylor, F. H. Davies, and S. P. Hepplestone, First principles electronic and elastic properties of fresnoite Ba2TiSi2O8, Mater. Res. Express **4**, 125904 (2017).
[20] R. Hanus, J. George, M. Wood, Y. Cheng, D. E. Abernathy, M. E. Manley, G. Hautier, G. Snyder, and R. P. Hermann, Uncovering design principles for amorphous-like heat conduction using two-channel lattice dynamics, Mater. Today Phys. **18**, 100344 (2021).

[21] M. Simoncelli, N. Marzari, and F. Mauri, Unified theory of thermal transport in crystals and disordered solids, Nat. Phys. **15**, 109 (2019).

[22] M. B. Stone, J. L. Niedziela, D. L. Abernathy, L. DeBeer-Schmitt, G. Ehlers, O. Garlea, G. E. Granroth, M. Graves-Brook, A. I. Kolesnikov, A. Podlesnyak, and B. Winn, A comparison of four direct geometry time-of-flight spectrometers at the spallation neutron source, Rev. Sci. Instrum. **85**, 045113 (2014).

[23] R. T. Azuah, L. R. Kneller, Y. Qiu, P. L. W. Tregenna-Piggott, C. M. Brown, J. R. D. Copley, and R. M. Dimeo, DAVE: A comprehensive software suite for the reduction, visualization, and analysis of low energy neutron spectroscopic data, J. Res. Natl. Inst. Stand. Technol. **114**, 341 (2009).

[24] See Supplemental Material at http://link.aps.org/supplemental/10.1103/PhysRevLett.129.255901 for a description of resolution correction details for HYSPEC, factors contributing to the mode specific thermal conductivities, and an estimate of the phason thermal conductivity directly from dispersion measurements.

[25] G. Nilsson and G. Nelin, Phonon dispersion relations in Ge at 80 K, Phys. Rev. B **3**, 364 (1971).

[26] D. L. Abernathy, M. B. Stone, M. J. Loguillo, M. S. Lucas, O. Delaire, X. Tang, J. Y. Y. Lin, and B. Fultz, Design and operation of the wide angular-range chopper spectrometer ARCS at the Spallation Neutron Source, Rev. Sci. Instrum. **83**, 015114 (2012).

[27] G. L. Squires, *Introduction to the Theory of Neutron Scattering* (Cambridge University Press, Cambridge, England, 1978), pp. 30–60.

[28] M. E. Manley, R. J. McQueeney, B. Fultz, R. Osborn, G. H. Kwei, and P. D. Bogdanoff, Vibrational and electronic entropy of β-cerium and γ-cerium measured by inelastic neutron scattering, Phys. Rev. B **65**, 144111 (2002).

[29] J. Y. Lin, F. Islam, and M. Kresh, Multiphonon: Phonon density of states tools for inelastic neutron scattering powder data, J. Open Source Software **3**, 440 (2018).

[30] C. Kittel, *Introduction to Solid State Physics*, 7th ed. (Wiley, New York, 1996), p. 117.

[31] R. J. Hardy, Energy-flux operator for a lattice, Phys. Rev. **132**, 168 (1963).

[32] P. B. Allen and J. Feldman, Thermal conductivity of disordered harmonic solids, Phys. Rev. B **48**, 12581 (1993).

[33] L. Isaeva, G. Barbalinardo, D. Donadio, and S. Baroni, Modeling heat transport in crystals and glasses from a unified lattice-dynamical approach, Nat. Commun. **10**, 3853 (2019).

[34] Y. Luo, X. Yang, T. Feng, J. Wang, and X. Ruan, Vibrational hierarchy leads to dual-phonon transport in low thermal conductivity crystals, Nat. Commun. **11**, 2554 (2020).